Research Square

Preprints are preliminary reports that have not undergone peer review.
They should not be considered conclusive, used to inform clinical practice,
or referenced by the media as validated information.

BRD4/H3K27Ac Epigenetic Reprogramming Orchestrates Chemotherapy-induced Polyploid Giant Cancer Cells and Glioma Progression

Jinlong Shi

shij@ntu.edu.cn

Department of Neurosurgery, Affiliated Hospital of Nantong University https://orcid.org/0009-0000-9308-2807

Yan Song

Affiliated Hospital of Nantong University

Jiabing Shen

Affiliated Hospital of Nantong University

Xuyou Zhang

Affiliated Hospital of Nantong University

Chunbing Shao

Affiliated Hospital of Nantong University

Yue Huang

Affiliated Hospital of Nantong University

Zhijie Feng

Affiliated Hospital of Nantong University

Zhengqiang Wan

Yancheng City No.1 People's Hospital

Jianhong Shen

Affiliated Hospital of Nantong University

Article

Keywords: glioma, chemoresistance, polyploid giant cancer cells, epigenetic reprogramming, BRD4, cancer stem cells

Posted Date: May 19th, 2026

DOI: https://doi.org/10.21203/rs.3.rs-9526893/v1

License: This work is licensed under a Creative Commons Attribution 4.0 International License.
Read Full License

Additional Declarations: (Not answered)

Abstract

Glioma chemoresistance is a primary driver of disease recurrence and poor patient survival. In this study, we demonstrate for the first time that glioma resistance to temozolomide (TMZ) is directly linked to the formation of polyploid giant cancer cells (PGCCs), both *in vivo* and *in vitro*. The prevalence of PGCCs is progressively increased with glioma stage and predicts unfavorable clinical outcomes. Notably, PGCCs showed markedly enhanced tumorigenicity, invasiveness, and chemoresistance, compared with parental glioma cells. Integrated RNA-seq and CUT&Tag profiling traced these aggressive traits to profound epigenetic reprogramming, characterized by expanded BRD4 and H3K27Ac chromatin occupancy and consequent activation of downstream oncogenic pathways. Accordingly, targeting this epigenetic state with Bromodomain and Extra-Terminal domain inhibitors (BETi) diminished PGCC-associated stemness, invasion, and chemoresistance. Moreover, we identified Tyrosine kinase with Immunoglobulin-like and EGF-like domains 1 (TIE1) as a novel, PGCC-specific transcriptional target of BRD4/H3K27Ac axis. Silencing TIE1 abolished the cancer stem cell (CSC)-like phenotype, invasiveness, and chemoresistance of PGCCs by inhibiting the PI3K/AKT/GSK3β/β-catenin pathway. Collectively, this study defines PGCC formation and its accompanying BRD4/H3K27Ac-driven epigenetic reprogramming as a pivotal mechanism of glioma chemoresistance, nominating BET targeting as a promising synergistic therapeutic strategy.

INTRODUCTION

Glioma is the most frequent malignant brain tumor, accounting for 75% of cases in grow-ups, with an immensely high recurrence rate and mortality [1]. Glioblastoma (GBM), the most aggressive form, has a median patient survival of approximately 15 months [2]. Although chemotherapy remains the most effective non-invasive treatment, resistance to frontline chemotherapeutic agents poses a major clinical challenge [3, 4]. The molecular mechanisms underlying glioma chemoresistance involve a range of complex cellular and molecular alterations, including the presence of cancer stem cells (CSCs), dysregulated metabolism, changes in the tumor microenvironment (TME), and epigenetic modifications [5, 6]. Stress induced by standard chemotherapeutic agents such as temozolomide (TMZ), a DNA-alkylating agent, may further promote tumor evolution and resistance. A more comprehensive understanding of the phenotypic and molecular changes driving these processes is essential for enhancing the efficacy of glioma therapy.

Accumulating data indicate that polyploid giant cancer cells (PGCCs) play a critical role in tumor progression due to their unique biological features. Unlike regular-sized diploid cancer cells, PGCCs contain either a highly enlarged nucleus or multiple nuclei, often accompanied by markedly increased cell size [7, 8]. These cells have been increasingly recognized across a variety of solid tumors and exhibit hallmark features, such as cancer stem cell (CSC)-like traits and enhanced resistance to therapeutic stress [8–13]. Studies have implicated hyperactivated oncogenic signaling and epigenetic dysregulation in the formation and maintenance of PGCCs [14, 15]. However, the functional relevance and clinical significance of PGCCs in glioma remain largely unexplored and warrant further investigation.

Our present study uncovered a close association between glioma chemoresistance and PGCC formation, and identified a critical role for the BRD4/H3K27Ac epigenetic regulation in this process. H3K27Ac is an epigenetic mark that defines super-enhancer (SE) regions and drives hyperactive transcription of target genes through extended cis-regulatory mechanisms[16]. Bromodomain and Extra-Terminal domain (BET) family proteins, particularly BRD4, serve as key readers of SEs and have been widely implicated in promoting malignant phenotypes by facilitating SE-driven transcriptional enhancements [17]. The BRD4/H3K27Ac axis plays a pivotal role in sustaining cancer stem cell (CSC) properties, promoting metastasis, and conferring resistance to chemotherapy, primarily through the transcriptional upregulation of oncogenic drivers, such as Myc, CCND1, BCL-2, IL-6, and SOX9 [18–20]. Beyond these established effectors, the list of oncogenic targets downstream of this pathway continues to grow, solidifying its status as a master regulator of cancer [21]. Notably, multiple BET inhibitors (BETi) have shown encouraging anti-tumor activity in clinical trials for advanced cancers [16, 22], underscoring their potential as effective components of combinatorial therapeutic strategies against glioma and other aggressive malignancies.

In this study, we identified the formation of PGCCs as a key mechanism driving glioma resistance to TMZ both *in vitro* and *in vivo* models. Transcriptomic and epigenetic analyses revealed that hyperactivation of the BRD4/H3K27Ac signaling axis underpins PGCC formation and their malignant behaviors. Pharmacological inhibition of BET proteins markedly suppressed PGCC-associated cancer stemness, invasiveness, and chemoresistance. Furthermore, we identified the TIE1/PI3K/AKT/GSK3β/β-catenin pathway as a novel downstream effector of BRD4/H3K27Ac signaling and demonstrated that its blockade effectively attenuates PGCC-driven malignancy. Altogether, our findings highlight a pivotal role for PGCCs and BRD4/H3K27Ac hyperactivation in glioma chemoresistance and suggest that combinatorial targeting of the BET pathway represents a promising therapeutic strategy to overcome resistance in glioma.

RESULTS

Chemotherapy-resistant PGCCs in glioma contributes to tumor progression

To investigate the clinical relevance of polyploid giant cancer cells (PGCCs) in glioma progression, we analyzed their presence in a clinical cohort of 203 glioma patients. We confirmed the presence of PGCCs, defined as cells with irregularly giant or multiple nuclei (Fig. 1A and 1B). Notably, PGCC numbers increased progressively with tumor grade, suggesting their involvement in glioma malignancy and disease advancement (Fig. 1C). Furthermore, PGCC abundance was inversely correlated with recurrence-free survival (Fig. 1D). Kaplan-Meier analysis revealed significantly worsened overall survival in patients with high PGCC levels compared to those with low PGCC levels in grade III and IV (Fig. 1E). These findings highlight PGCCs as a clinically relevant subpopulation associated with disease progression in glioma.

Given the strong association between PGCC abundance and glioma progression, we hypothesized that therapeutic interventions may influence PGCC accumulation. Specifically, based on the established link between PGCCs and cellular stress environments, we proposed that PGCC formation is associated with therapy-induced stress, such as exposure to temozolomide (TMZ) [23]. To investigate this causal relationship, we established TMZ-exposed models using glioma cell lines and xenograft animals. TMZ exposure dose-dependently reduced the viability of U87 and U251 cells, with IC50 values ranging from 1 to 3 mM (Fig. 2A). The experimental design is shown in Fig. 2B. Upon TMZ treatment followed by drug withdrawal, we observed a marked increase in cell size in the remaining populations, particularly at day 14 (Figs. 2C). DAPI staining revealed a high incidence of polyploidy, indicating the emergence of PGCCs (Fig. 2D). This was further supported by flow cytometry, which showed an elevated proportion of cells with polyploid DNA content (Figs. 2E and 2F). Interestingly, the PGCC population declined dramatically from day 14, probably due to the generation of diploid daughter cells[24]. Notably, PGCCs were also abundantly detected in TMZ-treated xenograft tumors, suggesting that PGCCs formation is a general adaptive mechanism contributing to TMZ resistance in glioma (Fig. 2G and 2H).

PGCCs exhibit CSC-like traits, enhanced invasiveness, and chemoresistance

To clarify the molecular features of PGCCs, we compared the expression of oncogenic markers between PGCCs and normally cultured glioma cells. Western blot analysis revealed marked upregulation of stemness-associated proteins in PGCCs, including CD133, Nestin, SOX2, and CD15 (Figs. 3A and 3B). Consistently, flow cytometry demonstrated a significantly increased proportion of $CD133^{+}$ CSC-like cells within the PGCC population (Figs. 3C and 3D). In support of these findings, PGCCs showed an enhanced capacity to form CSC-like spheres (Supplementary Fig. 1).

Given that GBM CSCs has been closely linked to metastatic and chemo-resistant properties, we next evaluated these phenotypes in PGCCs [25, 26]. Matrigel transwell assays demonstrated greater invasive capacity in PGCCs compared with their parental glioma counterparts (Supplementary Fig. 2). In line with these findings, PGCCs displayed multidrug resistance, showing increased tolerance to TMZ, Irinotecan, Carmustine, and Cisplatin (Supplementary Fig. 3). To further assess the tumorigenic potential, both U87-PGCCs and parental U87 cells were implanted into xenograft models. PGCC-derived tumors exhibited markedly accelerated growth and progression (Figs. 3E and 3F; Supplementary Fig. 4A). Immunohistochemical analysis further revealed elevated expression of the proliferation marker Ki-67 and the stemness marker SOX2 in PGCC-derived xenografts (Supplementary Figs. 4B and 4C).

The occurrence of BRD4/H3K27Ac epigenetic reprogramming in TMZ treatment-derived PGCCs

To systemically characterize the molecular alterations underlying PGCC formation, differential transcriptomic profiles were investigated using RNA-sequencing (RNA-seq) analysis. PGCCs displayed

distinct RNA expression profiles, compared with their parental counterparts (Supplementary Fig. 5A). Significant upregulation of genes involved in cell stemness (*MYC*, *NANOG*), proliferation (*CCND1, CCND2*), survival (*BCL2A1*) and pro-inflammatory secretion (*CCL3*, *IL1B*) were observed (Fig. 4A). GSEA analysis uncovered strong enrichments in E2F, MYC and G2M pathways and deprivation of TP53 and apoptosis pathways (Fig. 4B and Supplementary Fig. 5B). Because of a critical influence of these pathways by BRD4 inhibitors in GBM, we hypothesized a role of BRD4/H3K27Ac epigenetic reprogramming in driving PGCC-associated molecular alterations [27–29] .

To validate this hypothesis, BRD4 and H3K27Ac epigenetic profiles were assessed using the CUT&Tag technique. We observed significantly increased chromatin enrichment for the H3K27Ac marker and BRD4 binding in PGCCs (Fig. 4C). Systemic investigations revealed significantly increased upregulation of peaks (mean score FC > 1.5) in both BRD4 and H3K27Ac occupancy (Fig. 4D).

Notably, when examining downstream target genes, we found varying degrees of upregulation in BRD4/H3K27Ac enrichment. BRD4/H3K27Ac binding at well-documented gene loci, such as *MYC* and *CD274*, was largely unchanged (Supplementary Fig. 5C). In contrast, BRD4/H3K27Ac enrichment in the loci of glioma-promoting genes, such as *CDK18* and *SOX9*, exhibited substantial upregulation in PGCCs (Fig. 4E). Notably, BRD4 and H3K27Ac co-occupancy emerged at targets such as *CCL3* and *NANOG* in PGCCs, but barely observed in parental glioma cells (Fig. 4E). To examine the involvement of BRD4/H3K27Ac occupancy in gene transcription following PGCC formation, we analyzed peak profiles in PGCC upregulated genes. Within a total of 3348 upregulated genes in PGCCs (logFC > 1 and FDR < 0.05), 1843 genes (50.96%) show BRD4/H3K27Ac co-occupancy in PGCC cells (Fig. 4F). Among them, 71.78% of the genes possess peaks showing notable increase in BRD4/H3K27Ac co-occupancy (Up), and de novo BRD4/H3K27Ac peaks (De_novo) were identified in 12.32% genes, highlighting a connection between altered BRD4/H3K27Ac peaks and PGCC-associated gene transcription (Fig. 4G). These findings suggest that BRD4/H3K27Ac epigenetic markers are variably enhanced in gene loci and critically implicated in gene transcription in PGCCs.

BET inhibitor treatment diminishes PGCC-associated CSC-like traits, invasiveness, and chemoresistance

To determine whether BRD4/H3K27Ac epigenetic reprogramming drives PGCC aggressiveness, we first compared the expression of BRD4 and H3K27Ac in control versus TMZ-treated tumors. Both markers were strongly upregulated in TMZ-exposed xenograft tumors, particularly within PGCCs, relative to controls (Supplementary Fig. 6). These results confirm a general hyperactivation of BRD4/H3K27Ac epigenetic marks in TMZ-induced PGCCs. Next, we employed several BET inhibitors (BETi) tested in clinical trials, including I-BET-762 and Pelabresib. Co-treatment with these BETi sensitized PGCCs to standard glioma chemotherapeutics such as temozolomide (TMZ) and carmustine (Figs. 5A and 5B). Importantly, BETi treatment markedly impaired the sphere-forming capacity of PGCCs, indicative of reduced stem-like properties (Figs. 5C and 5D). Transwell assays further revealed that BETi exposure

significantly suppressed PGCC migration and invasion (Figs. 5E and 5F). Together, these findings demonstrate that pharmacological inhibition of BET proteins effectively attenuates the malignant phenotypes of PGCCs, underscoring their therapeutic potential in overcoming TMZ-induced chemoresistance.

TIE1 atypical oncogenic pathway is activated by BRD4/H3K27Ac axis and contributes to PGCC malignancy

Because of the occurrence of novel BRD4/H3K27Ac co-occupancy peaks in PGCCs, we investigated potential downstream targets of this epigenetic reprogramming. RNA-seq analysis revealed top upregulated genes in PGCCs, among which CCL3, TIE1, SPRR2D, RGS16, MMP10 and NANOG exhibited prominent de novo BRD4/H3K27Ac binding peaks (Figs. 6A). RT-qPCR analysis verified the upregulation of top genes identified from RNA-seq data (Fig. 6B). Furthermore, using western blot analysis, we confirmed that TIE1 and MYC proteins were substantially upregulated in PGCCs, compared with parental glioma cells (Fig. 6C). In addition to TMZ-induced models, we also observed significant upregulation of TIE1 in cisplatin-initiated PGCCs, indicating that TIE1 expression represents a general PGCC-specific target in glioma (Supplementary Fig. 7). Notably, multiple de novo BRD4/H3K27Ac peaks were exclusively identified in TIE1 gene loci in PGCCs, underscoring a potential link between BRD4/H3K27Ac co-occupancy and TIE1 expression (Fig. 6D). Accordingly, treatment with BET inhibitors reduced TIE1 expression in PGCCs, supporting a causal role for BRD4/H3K27Ac axis in its transcriptional activation (Fig. 6E).

While TIE1 is widely recognized as a pro-angiogenic tyrosine kinase receptor primarily expressed in endothelial cells, it has also been reportedly implicated in CSC properties and metastatic phenotypes within cancer cells [29–31]. To examine the function of TIE1 in PGCC phenotypes, we silenced TIE1 expression and assessed its downstream signaling pathways. Consistent with previous reports, western blot analysis showed that TIE1 depletion led to the attenuation of PI3K/AKT pathway (Fig. 7A) [30, 31]. Moreover, the downstream GSK3β/β-catenin axis, a crucial signaling implicated in GBM stemness, metastasis and chemoresistance, was significantly impaired following TIE1 silencing (Fig. 7A). In supporting of these findings, TIE1 depletion also resulted in decreased expression of stem markers CD133 and SOX2 (Figs. 7B and 7C).

Next, we evaluated the role of TIE1 in malignant behaviors of PGCCs. In vitro assays confirmed that TIE1 knockdown impaired CSC sphere formation, transwell invasiveness, and chemoresistance in PGCCs (Supplementary Fig. 8). Consistently, TIE1 depletion caused dramatically suppressed tumor growth in xenograft models (Figs. 7D and 7E). Accordingly, mice implanted with TIE1-silenced PGCCs showed significantly prolonged survival (Fig. 7F). These data demonstrate that, similar to BET inhibition, targeting TIE1 substantially impairs the tumorigenic potential of TMZ-induced PGCCs.

DISCUSSION

Currently, the standard treatment for glioma includes maximal safe surgical resection followed by concurrent radiotherapy and chemotherapy especially TMZ[32]. However, despite initial responses, tumor recurrence is almost inevitable, primarily due to the development of chemoresistance[33]. In this study, we identified PGCC formation and its associated epigenetic reprogramming as key mechanisms driving TMZ resistance in glioma. Specifically, we demonstrated that the BRD4/H3K27Ac epigenetic axis and its downstream TIE1/PI3K/AKT/GSK3β/β-catenin signaling pathway play pivotal roles in PGCC biology. Targeting these pathways effectively suppressed the aggressive phenotypes of PGCCs, underscoring their critical function in sustaining TMZ-induced PGCC formation and chemoresistance. Taken together, our findings highlight the central role of PGCCs and their epigenetic reprogramming in mediating TMZ resistance in glioma.

PGCCs have emerged as a distinct subpopulation that fuels tumor fitness and aggressiveness. Their formation is closely linked to tumor adaptation under stress conditions such as DNA damage, hypoxia, and nutrient deprivation[34–36]. PGCCs are commonly induced by chemotherapeutic agents, particularly microtubule-depolymerizing drugs like paclitaxel and docetaxel, likely due to their inhibition of cytokinesis[37, 38]. While PGCCs have been associated with immunosuppressive microenvironments and vasculogenesis in glioma[35, 39], their clinical significance remains poorly understood. Our study revealed widespread PGCC formation in glioma tumors as a general mechanism of resistance to frontline chemotherapy. Transcriptomic and bioinformatic analyses showed significant enrichment of oncogenic pathways such as MYC and E2F, while functional assays demonstrated that PGCCs possess enhanced cancer stem cell properties, increased invasiveness, and greater chemoresistance. Moreover, PGCCs exhibited marked upregulation of pro-inflammatory cytokine genes including *IL1A*, *IL1B*, *IL6*, *CXCL8*, and *CCL3*, suggesting additional roles in tumor progression that merit further investigation. These findings underscore PGCCs as key contributors to glioma aggressiveness beyond stress adaptation, emphasizing the need for their targeted elimination to achieve complete tumor eradication.

Although PGCCs were identified in primary tumors decades ago, their transcriptional and epigenetic features remain poorly characterized[34, 40]. Previous studies have linked PGCC formation to molecular changes involving HIF-1α, cytoplasmic SIRT1, and various miRNAs [12, 38, 41]. However, comprehensive molecular profiling is still lacking. Recent RNA-seq analysis revealed a functional role for cytoplasmic p21 in PGCCs from multiple cancer cell lines[42], consistent with our observations in TMZ-induced PGCCs, suggesting conserved molecular signatures. Similarly, Zeina Nehme et al. reported that PGCC formation correlates with increased EZH2 and Myc expression, partially aligning with our data[43]. In contrast, the epigenetic landscape of PGCCs has remained largely unexplored. Through integrated transcriptomic and CUT&Tag analyses, we identified BRD4/H3K27Ac signaling as a key epigenetic regulator of PGCC malignancy. Notably, BET inhibition markedly reduced PGCC-driven CSC formation, invasion, and chemoresistance, highlighting the potential of incorporating BETi into standard adjuvant therapy to improve the survival of glioma patients. The translational relevance of this approach is underscored by formal clinical trial assessments of the BETi trotabresib and birabresib (formerly OTX015/MK-8628), both of which penetrate the blood–brain barrier and are well tolerated in glioblastoma (GBM) patients [44, 45]. Additionally, novel BET inhibitors with brain penetration and potent

anti-GBM activity are currently under development and in preclinical trials [46]. Collectively, these findings suggest that pharmacologically targeting the BET pathway may selectively suppress PGCC aggressiveness, highlighting the combination of BET inhibitors with TMZ as an enhanced chemotherapeutic strategy against glioma.

Although PGCCs have traditionally been regarded as a tumor escape mechanism in response to stress, mounting data indicate they harbor distinct cellular and molecular alterations[23, 47]. TMZ treatment activates multiple stress-responsive pathways, including JNK, IKK/NF-κB, and reactive oxidative species (ROS) [48–50]. These alterations may enhance BRD4 expression, chromatin binding, and transcriptional activity via post-translational modifications (PTMs) and other mechanisms [51–53]. Furthermore, BRD4 and P300 may cooperatively facilitate H3K27Ac modification when recruited to enhancer regions [16, 54]. In turn, activation of the BRD4/H3K27Ac axis drives diverse oncogenic transcription programs by reshaping the epigenetic landscape, ultimately contributing to PGCC formation.

Using RNA-seq and qRT-PCR, we revealed dramatic upregulation of various genes in PGCCs, such as TIE1, CCL3, LCE1F, and SPRR2D. These genes were barely expressed in normal glioma cells at RNA level, but showed apparent expression in PGCCs. Notably, these genes were rarely linked to tumor aggressiveness itself. For example, TIE1 is primarily expressed in endothelial cells and is best known for its role in angiogenesis[55]. In our study, TIE1 expression was notably enriched in PGCCs but absent in standard glioma cell lines. Functional assays revealed that TIE1 depletion led to a significant reduction in PI3K/AKT/GSK3β/β-catenin signaling, suggesting a role in promoting glioma malignancy. Consistently, TIE1 was critical for maintaining CSC-like properties, invasion, and chemoresistance in PGCCs. Furthermore, CUT&Tag analysis revealed TIE1 as a direct downstream target of BRD4/H3K27Ac, suggesting that epigenetic remodeling in PGCCs drives the activation of oncogenic programs. These findings support the notion that PGCC-associated epigenetic reprogramming may facilitate tumor aggressiveness through the induction of atypical oncogenic pathways.

Limitations of this study

This study has several limitations. First, although PGCC formation was apparently observed in glioma chemoresistance models both *in vivo* and *in vitro*, the mechanistic insights into their molecular and epigenetic alterations were derived exclusively from *in vitro* PGCC cultures. To enable comprehensive characterization of PGCCs within tumors, it is essential to overcome the technical challenges associated with isolating intact PGCCs from fresh primary tumors in a manner compatible with transcriptomic and epigenetic profiling. Secondary, while we explicitly revealed that BRD4/H3K27Ac was hyperactivated in TMZ-induced PGCCs, the mechanisms underpinning this epigenetic reprogramming remains obscure. Consistent with our findings, several studies have reported BRD4/H3K27Ac hyperactivation in chemoresistant cancer cells. However, the upstream drivers of this activation remain undefined and warrant further investigation[56–59]. Another limitation is the incomplete characterization of the BRD4/H3K27Ac pathway in glioma malignancy. While we identified the upregulation of BRD4 downstream effectors such as Myc, E2F, and TIE1 in PGCCs, many additional targets remain to be

elucidated. For instance, BRD4 may facilitate the expression of pro-inflammatory cytokines in PGCCs, suggesting a potential role in modulating the tumor immune microenvironment (TIME) and influencing immunotherapy efficacy. Moreover, although we confirmed a functional role for TIE1 in PGCCs, systematic investigation of BRD4-regulated downstream effectors remains lacking. Further studies are needed to fully delineate the contribution of epigenetic reprogramming to PGCC formation and glioma progression.

Conclusion

In conclusion, our study demonstrates that PGCC formation is a critical mechanism underlying glioma resistance to TMZ. Mechanistic analyses revealed a central role for BRD4/H3K27Ac-driven epigenetic reprogramming in driving PGCC formation and the associated aberrant transcriptomic landscape. TMZ-induced PGCCs exhibit strong CSC-like traits, invasive capacity, and chemoresistance. Importantly, pharmacological targeting of the BRD4 or TIE1 pathways significantly attenuated PGCC aggressiveness, underscoring their translational potential in overcoming TMZ resistance in glioma.

Materials and methods

Human Glioma specimens

A total of 203 glioma tumor samples were collected from two independent centers. Among them, 63 samples were collected from the Affiliated Hospital of Nantong University, all pathologically confirmed as glioma and approved by the hospital's ethics committee (ethics approval no. 2020-L001). The remaining 140 samples from human glioma tissue array were obtained from the National Engineering Center for Biochip (Cat# HBraG177Su01; Outdo Biotech, Shanghai, China) (ethics approval no. SHYJS-CP-1801002). Most patients enrolled received standard adjuvant therapy, including radiotherapy and/or chemotherapy, in accordance with the guidelines of the Chinese Glioma Cooperative Group (CGCG), the Society for Neuro-Oncology of China (SNO-China) and Chinese Brain Cancer Association (CBCA) [60]. All tissue samples underwent hematoxylin and eosin (HE) staining. The number of PGCCs in each tissue was independently and blindly evaluated by two histologists, and consensus was reached.

Cell culture and PGCCs formation

The human glioma cell lines U87 (RRID: CVCL_0022) and U251 (RRID: CVCL_0021) were obtained from the Cell Bank of the Chinese Academy of Sciences (Shanghai, China) in February 2023. Both lines were authenticated by short tandem repeat (STR) profiling and confirmed mycoplasma-free using the MycoFluor™ Mycoplasma Detection Kit (Thermo Fisher Scientific) prior to use. Cells were maintained in Dulbecco's modified Eagle's medium (DMEM; Gibco, Shanghai) supplemented with 10% FBS (Gibco) and 1% penicillin-streptomycin (Gibco) at 37°C in a humidified incubator with 5% CO_2 and 95% air. At 80% confluence, cells were treated with 3mM temozolomide (HY-17364, MedChemExpress) or 20μM cisplatin (HY-17394, MedChemExpress) for 16 hours and then allowed to recover for 10–14 days in regular

medium for PGCCs formation (replaced every 3 days). All experiments were conducted with cells within 10 passages after thawing.

Tumorsphere formation assays

U87, U251 and their derivative PGCCs cells were cultured in serum-free stem cell medium (DMEM/F12 medium; #10565042, Gibco) supplemented with 20 ng/ml EGF (#AF-100-15, Peprotech), 20 ng/ml bFGF (#AF-100-18B, Peprotech), 1% N2 (#17502-048, Gibco) and 2% B27 (#17504-044, Gibco) supplements. A total of 1×10^4 cells were seeded in 3 ml of stem cell medium in low-attachment 6-well plates (Corning). Tumorsphere (> 50 cells) numbers and sizes were calculated at the seventh day after cell placement. Each group was derived from three biologically independent replicates.

Animal procedures

6–8 weeks old male BALB/c nude mice weighing between 18-22g were used to establish the orthotopic glioma nude mouse model. The mice were purchased from the experimental animal center of Nantong University of China and housed in a specific pathogen–free (SPF) facility at the animal house of Nantong University under controlled conditions (22–24°C, 40–60% humidity, 12 h light/dark cycle) with free access to food and water in an enriched environment.

U87 cells were transduced with luciferase-expressing lentivirus (Genechem Co., Ltd. Shanghai) before tumor implantation. Mice were anesthetized with inhalation of 1–5% isoflurane (RWD, China). After the mice were subjected to deep anesthesia, they were positioned in a stereotactic fixation device (David Kopf Instruments, Tujunga, CA, USA). To compare the differences in tumor-forming capacity between PGCCs and parental glioma cells, $^{Luc+}$U87 and $^{Luc+}$U87-PGCCs cells (5×10^4 cells per mouse) were implanted in the right brains of mice (2.0mm lateral, 0.5mm anterior to the bregma, at a depth of 3mm) at a rate of 2 μL/minutes. The needle was left in place for an additional minute before being slowly withdrawn to prevent backflow. After the injection, the skin was disinfected and sutured. The mice were placed on a heating pad until full recovery from anesthesia. To minimize animal suffering, carprofen (5 mg/kg) and antibiotics were administered intraperitoneally for three consecutive days post-surgery. Animals were monitored daily for behavior, weight, and surgical wound recovery. Any animals exhibiting signs of severe distress or morbidity were humanely euthanized via CO_2 asphyxiation in accordance with the experimental protocol.

To assess the effect of TIE1 expression on the tumorigenesis of PGCCs, orthotopic tumor growth was monitored using a small animal live imaging system (IVIS Spectrum, USA) on day 8, 11, 14, and 17 after tumor implantation. Each model mouse was pre-injected with D-Luciferin potassium salt (150 mg/kg, APExBIO Technology, USA) to stimulate luciferase activity. The survival time of the mice in each group was observed, and the body weight of the mice was recorded every three days. All animal experiments were carried out in accordance with the Guide for the Care and Use of Laboratory Animals and approved by the Ethics Committee of Experimental Animal of Nantong University (approval no. S20240116-009).

Scoring for PGCCs

Tumor cells with highly enlarged nuclei at least three times larger than diploid cells or multiple nuclei were regarded as PGCCs[7, 8]. The maximal diameter of cell nuclei was measured using Zen and Image J software for this study. For each case, five representative microscopic fields were selected at ×200 magnification, and the total number of PGCCs was counted independently by two histologists blinded to clinical information. The average count per field was calculated, and patients were stratified into high- and low-PGCC groups based on the median value of PGCC counts across the cohort. Discrepancies between the two observers were resolved by consensus review.

Flow cytometry analysis

The genome content of the PGCCs cells was assessed using Propidium Iodide (PI; C1052, Beyotime). For each experiment, a total of 1 million cells were fixed in cold 70% ethanol for 4h. The cells were washed with PBS twice. The supernatant was discarded and the pellet was resuspended in PI (200 µL from 50 µg/mL stock) in PBS. The cells were stained for 20 min at room temperature in dark. Then, the cells were washed with PBS twice, resuspended in 500 uL PBS, and analyzed using Flow cytometry.

To investigate the expression of the stemness marker CD133 on the cell surface, a total of 1 million cells for each experiment cells were collected, washed with 1xPBS twice, and then incubated with FITC-conjugated anti-CD133antibody (W6B3C1, BioLegend) or APC-conjugated anti-CD133 antibody (S16015F, BioLegend) for 30 min at room temperature in dark. Then, the cells were washed with PBS twice, resuspended in 500uL 1xPBS, and analyzed using Flow cytometry.

All flow cytometry experiments were conducted on a FACSCalibur flow cytometer (BD Biosciences). Each dataset represents three independent biological replicates, and data were analyzed using FlowJo software (version 10.1).

RNA Isolation and Quantitative Real-Time PCR (qRT-PCR)

RNA was isolated using TRIzol reagent (Invitrogen) according to the manufacturer's protocol. cDNA was reverse transcribed using the RevertAid First Strand cDNA Synthesis kit (Thermo Fisher Scientific) and subjected to qRT-PCR analysis on an ABI QuantStudio5 Q5 real-time PCR system (Thermo Fisher Scientific) using SYBR Green master mix (Roche, Germany). The specific divergent primers were shown in Supplementary Table S1.

Cell migration and invasion assays

For the assessment of cell migration, 500 µL of medium containing 20% FBS was added to 24-well plates. Then, cells were resuspended in DMEM basal medium at a density of 1×10^4 cells/well and added to the transwell chambers (Corning), which were then placed in the plates. After 24 h-48h of culture, cells were fixed with 4% paraformaldehyde, and subjected to 0.1% crystal violet staining for 30 min. The staining results were visualized under a digital microscope (Leica DM3000) and five random non-overlapping fields of each well were analyzed for quantification.

For invasion assays, the cell density was adjusted to 2×10^4 cells/well. Matrigel (Corning) was mixed with the basal medium at a ratio of 1:7 and added to the upper chamber for 12 h. The remaining procedure was identical to the cell migration experiments.

Cell viability assessment and in vitro cytotoxicity assay

Cell viability was assessed using trypan blue staining assay. Single cell suspensions were mixed with 0.4% trypan blue staining (1:1) and then counted under a light microscope. At least 400 cells per group were counted, with four replicates per group (n = 4).

The cytotoxicity of the anticancer drugs on cells was assessed using the Cell Counting Kit-8 (CCK8) according to the manufacturer's protocol. Briefly, cells were seeded into 96-well plates at a density of 1×10^4cells/well. After cell adherence, cells were exposed to different concentrations of TMZ (HY-17364, MedChemExpress), Irinotecan (HY-16562, MedChemExpress), Carmustine (HY-13585, MedChemExpress,), and Cisplatin (HY-17394, MedChemExpress) for 16h. Thereafter, 10μl of CCK8 solution (C0039, Beyotime) was added to each well and incubated for an additional 1-2h. Optical density (OD) at 450nm was determined using spectrophotometric analysis (Thermo Scientific Multiskan®FC).

Western blot

Cell pellets were harvested using a cell scraper in adequate amounts of RIPA buffer (P0013B, Beyotime) supplemented with 1×protease inhibitor cocktail (PIC; #A32963, Thermo Fisher Scientific) and 1mM PMSF, and lysed on ice for 30 min. After centrifugation at 13 000 g, 4°C for 15 min, the supernatant was transferred and subjected to BCA protein assay (#23225, Thermo Fisher Scientific). An equal amount of proteins (30 μg) were separated on SDS-PAGE gels and transferred onto PVDF membranes (Amersham Bioscience). After blocking with 5% skimmed milk/TBST, the membranes were incubated with primary antibodies overnight at 4°C and then with HRP-conjugated secondary antibodies for 2h at room temperature. Protein signals were developed using an ECL (SQ201, Shanghai Epizyme Biomedical Technology Co., Ltd, Shanghai, China) kit and imaged on a gel scanning system (Tanon 5200 Multi, Shanghai, China) or ChemiDoc^{TM}MP Imaging System (Bio-Rad). Finally, protein quantification was performed using Image J software. The list of antibodies used in this study is presented in Supplementary Table S2.

Immunofluorescence

Cells were fixed with 4% paraformaldehyde, permeabilized with 1% Triton X-100 and blocked with 5% BSA. Thereafter, cell slides were incubated with primary antibody (rabbit anti-Tublin, SC-5286, Santa) overnight at 4°C, followed by Alexa Fluor-594-conjugated goat anti-rabbit IgG (Invitrogen) and DAPI (Invitrogen) counter staining. Fluorescence images were acquired using a confocal microscope (Zeiss, LSM900, Germany).

Immunohistochemistry

Tissue sections were deparaffinized through a graded ethanol series and subsequently treated with 3% H_2O_2 in methanol for 25 minutes at room temperature to quench endogenous peroxidase activity. After blocking with 3% bovine serum albumin (BSA) in PBS for 30 minutes, the sections were incubated overnight at 4°C in a humidified chamber with the following primary antibodies: Ki67 (27309-1-AP, Proteintech), and SOX2(#23064, CST). Thereafter, slides were washed three times with PBS and then incubated with horseradish peroxidase (HRP)-conjugated secondary antibodies for 50 minutes at room temperature. Immunoreactivity was developed using a 3,3'-diaminobenzidine (DAB) substrate kit. Finally, sections were counterstained with hematoxylin, dehydrated through an ascending ethanol series, cleared in xylene, and mounted with neutral balsam for microscopic evaluation. The immunostaining was quantified using the H-score (histochemical score) method. Briefly, the staining intensity was graded on a scale of 0–3 (0, negative; 1, weak; 2, moderate; 3, strong). The percentage of cells at each intensity level was determined by examining at least 500 cells per sample under high-power magnification (400×). The H-score was calculated as: ∑ (intensity score × percentage of cells at that intensity), yielding a possible range of 0 to 300. Scoring was performed in duplicate by two pathologists blinded to the sample identity.

shRNA transduction

The shRNAs targeting TIE1 were synthesized by Shanghai Genechem Co. Ltd (Shanghai, China) and subcloned into the pLKO.1 lentiviral construct. Lentiviral particles were produced in HEK293T cells using the helper plasmids pMD2.G and psPAX2. For knockdown experiments, PGCCs at 70% confluency were transduced with shTie1 or a non-targeting control shRNA (shNTC, 5’-CAA CAA GAT GAA GAG CAC CAA-3’) lentiviruses and selected with 2 μg/mL puromycin (ST551, Beyotime) for 48 hours. The sequences of Tie1-targeting shRNA are as follows: 5’-CTC TGA CTT AAG CTG CCT CAA-3’ and 5’-GCC TGT AAG AAC CGA GGT TAC-3’.

RNA sequencing and bioinformatics analysis

RNA sequencing (RNA-seq) and bioinformatics analysis were conducted by Shanghai Biotechnology Corporation (Shanghai, China). Briefly, total RNA was extracted using the RNeasy kit (#74104, Qiagen, Shanghai), qualified, and quantified, and subjected to RNA-seq on an Illumina Novaseq 6000 instrument (Illumina, USA) according to the manufacturer’s instructions. Sequence quality was assessed using FastQC, and the raw data were filtered with fastp to remove adaptors and low-quality bases. Next, clean reads were mapped to the human GRCh38 reference genome using Hisat2 and the raw read counts for each gene were obtained with featureCounts. Differentially expressed genes (DEGs) were identified with edgeR, applying thresholds of FDR < 0.05 and |fold change| ≥ 2.

CUT&Tag and data processing

CUT&Tag assay was performed using the Hyperactive Universal CUT&Tag Assay Kit (#TD904, Vazyme, Nanjing, China) according to the manufacturer’s protocol. Briefly, parental and derived PGCC cells were harvested with TrypLE and subjected to nuclear isolation using hypotonic method. Isolated nuclei were

resuspended in 100 μL Wash Buffer and bound to ConA Beads Pro. After one wash with 100 μL Binding Buffer, nuclei were resuspended in 50 μL Antibody Binding Buffer and incubated overnight at 4°C with 1 μg AbFlex anti-BRD4 antibody (#91301, Active Motif, Carlsbad, CA, USA) or AbFlex anti-H3K27Ac antibody (#91193, Active Motif). Nuclei were then incubated with secondary antibody (1:100 dilution) for 60 min at room temperature. After washing, nuclei were incubated with 0.04 μM pA/G-Tnp Pro in 100 μL Dig-300 Buffer for 1 h at room temperature, followed by DNA cleavage in the presence of Mg^{2+}. Released DNA was supplemented with 1 pg E. coli λ DNA spike-in, purified with DNA Extract Beads Pro, and subsequently PCR-amplified to generate sequencing libraries.

The raw sequencing data underwent initial quality assessment with FastQC, followed by adapter trimming and quality filtering using Cutadapt. The clean reads were then aligned to the human reference genome (hg38) with Bowtie2 using optimized parameters. Read counts were normalized based on the ratio of input nuclear DNA to spike-in λ DNA. Aligned reads were converted to bigWig format for visualization in the IGV browser, and enriched genomic regions were identified by peak calling with MACS2. Peak visualization, including heatmaps and density plots, was conducted on the Galaxy platform (https://usegalaxy.org/). To ensure specificity, subsequent analysis was restricted to BRD4 and H3K27Ac peaks that exhibited direct genomic overlap. From these, de novo peaks were identified as having a fold-change (FC) > 10 and a parental score < 10 for both factors. Other overlapping peaks demonstrating concurrent enrichment (FC > 1.5 for both BRD4 and H3K27Ac) were designated as upregulated.

Declarations

Ethics approval and consent to participate

The study was approved by the Ethics Committee of the Affiliated Hospital of Nantong University (approval no. 2020-L001). Ethical approval for the study of glioma tissue array was granted by the Outdo Biotech Clinical Research Ethics Committee (approval no. SHYJS-CP-1801002). All animal experiments were performed in accordance with the National Institutes of Health Guidelines for the Care and Use of Laboratory Animals and were approved by the Animal Ethics Committee of Nantong University (Approval No. S20240116-009).

Consent for publication

Not applicable

Availability of data and materials

RNA-seq, CUT&Tag data in this study are deposited in the NCBI SRA database with the accession of PRJNA1347817 and PRJNA1347786.

Competing interests

The authors declare no conflict of interest.

Acknowledgements
The authors thank the funding sources listed below. The funders had no role in study design, data collection, analysis, decision to publish, or preparation of the manuscript. No additional non-commercial materials were used in this study.

Funding

This study was supported by the Special Program of National Natural Science Foundation of China (T2541058), Jiangsu Provincial Natural Science Foundation (BK20251834), Nantong Natural Science Foundation(JC2025100), and Project of Nantong Commission of Health (MS2024001MS2025009).

Authors' contributions

Y Song, and JB Shen: Writing – review & editing, Writing – original draft, Validation, Software, Methodology, Data curation, Conceptualization. **XY Zhang, and CB Shao:** Software, Project administration, Methodology. **Y Huang, and ZJ Feng:** Validation, Software, Formal analysis. **ZQ Wan, JH Shen, and JL Shi:** Writing – review & editing, Supervision, Project administration, Funding acquisition, Data curation, Conceptualization.

Statistical analyses

Statistical differences were analyzed using GraphPad Prism8 software. All data were expressed as mean± SD. One-way analysis of variance (ANOVA) was used to compare multiple variables, followed by post hoc comparisons. Two-way ANOVA was conducted to analyze statistical differences in tumor growth and cytotoxicity assays between control and PGCC groups. T-tests were applied for two-group comparisons. $p < 0.05$ was considered statistically significant. Statistical significance was presented as follow: *, $p < 0.05$; **, $p < 0.01$; ***, $p < 0.001$; ****, $p < 0.0001$; ns, not significant.

References

1. Lapointe, S., A. Perry, and N.A. Butowski, Primary brain tumours in adults. Lancet, 2018. 392(10145): p. 432–446.
2. Dhingra, S., M. Koshy, and M. Korpics, Limited survival benefit in patients diagnosed with glioblastoma post-2016: a SEER population based registry analysis. J Cancer Res Clin Oncol, 2025. 151(6): p. 179.
3. Wu, H., et al., Modulation of blood-brain tumor barrier for delivery of magnetic hyperthermia to brain cancer. J Control Release, 2023. 355: p. 248–258.
4. Yalamarty, S.S.K., et al., Mechanisms of Resistance and Current Treatment Options for Glioblastoma Multiforme (GBM). Cancers (Basel), 2023. 15(7).

5. Jin, X., et al., RELL1, a novel oncogene, accelerates tumor progression and regulates immune infiltrates in glioma. Int Immunopharmacol, 2020. 87: p. 106707.
6. Singh, N., et al., Mechanisms of temozolomide resistance in glioblastoma - a comprehensive review. Cancer Drug Resist, 2021. 4(1): p. 17–43.
7. Liu, J., J. Erenpreisa, and E. Sikora, Polyploid giant cancer cells: An emerging new field of cancer biology. Semin Cancer Biol, 2022. 81: p. 1–4.
8. Zhang, S., et al., Generation of cancer stem-like cells through the formation of polyploid giant cancer cells. Oncogene, 2014. 33(1): p. 116–28.
9. You, B., et al., AMPK-mTOR-Mediated Activation of Autophagy Promotes Formation of Dormant Polyploid Giant Cancer Cells. Cancer Res, 2022. 82(5): p. 846–858.
10. Zhang, X., et al., Targeting polyploid giant cancer cells potentiates a therapeutic response and overcomes resistance to PARP inhibitors in ovarian cancer. Sci Adv, 2023. 9(29): p. eadf7195.
11. Mittal, K., et al., Multinucleated polyploidy drives resistance to Docetaxel chemotherapy in prostate cancer. Br J Cancer, 2017. 116(9): p. 1186–1194.
12. Lopez-Sanchez, L.M., et al., CoCl2, a mimic of hypoxia, induces formation of polyploid giant cells with stem characteristics in colon cancer. PLoS One, 2014. 9(6): p. e99143.
13. Sirois, I., et al., A Unique Morphological Phenotype in Chemoresistant Triple-Negative Breast Cancer Reveals Metabolic Reprogramming and PLIN4 Expression as a Molecular Vulnerability. Mol Cancer Res, 2019. 17(12): p. 2492–2507.
14. Niu, N., I. Mercado-Uribe, and J. Liu, Dedifferentiation into blastomere-like cancer stem cells via formation of polyploid giant cancer cells. Oncogene, 2017. 36(34): p. 4887–4900.
15. Liu, J., The dualistic origin of human tumors. Semin Cancer Biol, 2018. 53: p. 1–16.
16. Qian, H., et al., Super-enhancers and the super-enhancer reader BRD4: tumorigenic factors and therapeutic targets. Cell Death Discov, 2023. 9(1): p. 470.
17. Xu, F., et al., Bromodomain protein 4 mediates the roles of TGFbeta1-induced Stat3 signaling in mouse liver fibrogenesis. Toxicol Lett, 2023. 385: p. 42–50.
18. Dawson, M.A., et al., Inhibition of BET recruitment to chromatin as an effective treatment for MLL-fusion leukaemia. Nature, 2011. 478(7370): p. 529–33.
19. Durall, R.T., et al., The BRD4-NUT Fusion Alone Drives Malignant Transformation of NUT Carcinoma. Cancer Res, 2023. 83(23): p. 3846–3860.
20. Lockwood, W.W., et al., Sensitivity of human lung adenocarcinoma cell lines to targeted inhibition of BET epigenetic signaling proteins. Proc Natl Acad Sci U S A, 2012. 109(47): p. 19408–13.
21. Teng, X., et al., Super-enhancer inhibitors THZ2 and JQ1 reverse temozolomide resistance in glioblastoma by suppressing SE-driven SOX9 expression. Cancer Drug Resist, 2025. 8: p. 37.
22. Shukla, S., et al., BET inhibitors reduce tumor growth in preclinical models of gastrointestinal gene signature-positive castration-resistant prostate cancer. J Clin Invest, 2025. 135(16).

23. Song, Y., et al., Stress-Induced Polyploid Giant Cancer Cells: Unique Way of Formation and Non-Negligible Characteristics. Front Oncol, 2021. 11: p. 724781.
24. Zhao, Q., et al., High Migration and Invasion Ability of PGCCs and Their Daughter Cells Associated With the Nuclear Localization of S100A10 Modified by SUMOylation. Front Cell Dev Biol, 2021. 9: p. 696871.
25. Liu, T., et al., Circulating Glioma Cells Exhibit Stem Cell-like Properties. Cancer Res, 2018. 78(23): p. 6632–6642.
26. Niechi, I., et al., Cancer Stem Cell and Aggressiveness Traits Are Promoted by Stable Endothelin-Converting Enzyme-1c in Glioblastoma Cells. Cells, 2023. 12(3).
27. Xu, L., et al., Targetable BET proteins- and E2F1-dependent transcriptional program maintains the malignancy of glioblastoma. Proc Natl Acad Sci U S A, 2018. 115(22): p. E5086-E5095.
28. Ma, L., et al., An inhibitor of BRD4, GNE987, inhibits the growth of glioblastoma cells by targeting C-Myc and S100A16. Cancer Chemother Pharmacol, 2022. 90(6): p. 431–444.
29. He, Y., et al., Enhanced anti-glioma efficacy of doxorubicin with BRD4 PROTAC degrader using targeted nanoparticles. Mater Today Bio, 2022. 16: p. 100423.
30. Wei, Y., et al., Cervical cancer cell-derived Tie1 expression via PI3K/AKT signaling pathway promotes tumor progression. Exp Cell Res, 2024. 439(1): p. 114060.
31. Chen, E., et al., FLI1 regulates radiotherapy resistance in nasopharyngeal carcinoma through TIE1-mediated PI3K/AKT signaling pathway. J Transl Med, 2023. 21(1): p. 134.
32. Adegboyega, G., et al., Global Landscape of Glioblastoma Multiforme Management in the Stupp Protocol Era: Systematic Review Protocol. Int J Surg Protoc, 2021. 25(1): p. 108–113.
33. Goenka, A., et al., The Many Facets of Therapy Resistance and Tumor Recurrence in Glioblastoma. Cells, 2021. 10(3).
34. Illidge, T.M., et al., Polyploid giant cells provide a survival mechanism for p53 mutant cells after DNA damage. Cell Biol Int, 2000. 24(9): p. 621–33.
35. Liu, Y., et al., Hypoxia-induced polypoid giant cancer cells in glioma promote the transformation of tumor-associated macrophages to a tumor-supportive phenotype. CNS Neurosci Ther, 2022. 28(9): p. 1326–1338.
36. Mukherjee, S., et al., Mutation in SF3B1 gene promotes formation of polyploid giant cells in Leukemia cells. Med Oncol, 2022. 39(5): p. 65.
37. Zhao, S., et al., IL-1beta is involved in docetaxel chemoresistance by regulating the formation of polyploid giant cancer cells in non-small cell lung cancer. Sci Rep, 2023. 13(1): p. 12763.
38. Xu, H., et al., Cytoplasmic SIRT1 promotes paclitaxel resistance in ovarian carcinoma through increased formation and survival of polyploid giant cancer cells. J Pathol, 2023. 261(2): p. 210–226.
39. Qu, Y., et al., Number of glioma polyploid giant cancer cells (PGCCs) associated with vasculogenic mimicry formation and tumor grade in human glioma. J Exp Clin Cancer Res, 2013. 32(1): p. 75.

40. Andersson, G., Accumulation of polyploid cells and G2-phase cells during ascites tumor growth. J Cell Physiol, 1977. 90(2): p. 329–35.
41. Wang, L., et al., miR-1246 enhances chemo-resistance of polyploid giant cancer cells in H1299 cells by targeting GSK3beta/beta-catenin. Discov Oncol, 2025. 16(1): p. 901.
42. White-Gilbertson, S., et al., Transcriptome analysis of polyploid giant cancer cells and their progeny reveals a functional role for p21 in polyploidization and depolyploidization. J Biol Chem, 2024. 300(4): p. 107136.
43. Nehme, Z., et al., Polyploid giant cancer cells, EZH2 and Myc upregulation in mammary epithelial cells infected with high-risk human cytomegalovirus. EBioMedicine, 2022. 80: p. 104056.
44. Duan, W., M. Yu, and J. Chen, BRD4: New hope in the battle against glioblastoma. Pharmacol Res, 2023. 191: p. 106767.
45. Moreno, V., et al., Trotabresib, an oral potent bromodomain and extraterminal inhibitor, in patients with high-grade gliomas: A phase I, "window-of-opportunity" study. Neuro Oncol, 2023. 25(6): p. 1113–1122.
46. Jermakowicz, A.M., et al., The novel BET inhibitor UM-002 reduces glioblastoma cell proliferation and invasion. Sci Rep, 2021. 11(1): p. 23370.
47. Bhartiya, D., et al., Do PGCCs in Solid Tumors Appear Due to Treatment-related Stress or Clonal Expansion of CSCs that Survive Oncotherapy? Stem Cell Rev Rep, 2025. 21(5): p. 1594–1606.
48. Thanh, H.D., et al., Temozolomide promotes matrix metalloproteinase 9 expression through p38 MAPK and JNK pathways in glioblastoma cells. Sci Rep, 2024. 14(1): p. 14341.
49. Caporali, S., et al., NF-kappaB is activated in response to temozolomide in an AKT-dependent manner and confers protection against the growth suppressive effect of the drug. J Transl Med, 2012. 10: p. 252.
50. Li, H., et al., Overcoming temozolomide resistance in glioma: recent advances and mechanistic insights. Acta Neuropathol Commun, 2025. 13(1): p. 126.
51. Devaiah, B.N., et al., Phosphorylation by JNK switches BRD4 functions. Mol Cell, 2024. 84(22): p. 4282–4296 e7.
52. Pecharroman, I., et al., IkappaB kinase-alpha coordinates BRD4 and JAK/STAT signaling to subvert DNA damage-based anticancer therapy. EMBO J, 2023. 42(21): p. e114719.
53. Zhang, W., et al., Targeting BRD4 bromodomains and beyond: exploring new therapeutic frontiers. Trends Pharmacol Sci, 2026. 47(1): p. 15–39.
54. Wu, T., Y.F. Kamikawa, and M.E. Donohoe, Brd4's Bromodomains Mediate Histone H3 Acetylation and Chromatin Remodeling in Pluripotent Cells through P300 and Brg1. Cell Rep, 2018. 25(7): p. 1756–1771.
55. Yang, P., et al., Tie-1: A potential target for anti-angiogenesis therapy. J Huazhong Univ Sci Technolog Med Sci, 2015. 35(5): p. 615–622.

56. Shang, S., et al., Chemotherapy-Induced Distal Enhancers Drive Transcriptional Programs to Maintain the Chemoresistant State in Ovarian Cancer. Cancer Res, 2019. 79(18): p. 4599–4611.
57. Lusby, R., et al., Decoding gene regulatory circuitry underlying TNBC chemoresistance reveals biomarkers for therapy response and therapeutic targets. NPJ Precis Oncol, 2024. 8(1): p. 64.
58. Lee, J., et al., Pharmacologic Targeting of Histone H3K27 Acetylation/BRD4-dependent Induction of ALDH1A3 for Early-phase Drug Tolerance of Gastric Cancer. Cancer Res Commun, 2024. 4(5): p. 1307–1320.
59. Ranjit, M., et al., Aberrant Active cis-Regulatory Elements Associated with Downregulation of RET Finger Protein Overcome Chemoresistance in Glioblastoma. Cell Rep, 2019. 26(9): p. 2274–2281 e5.
60. Jiang, T., et al., Clinical practice guidelines for the management of adult diffuse gliomas. Cancer Lett, 2021. 499: p. 60–72.

Figures

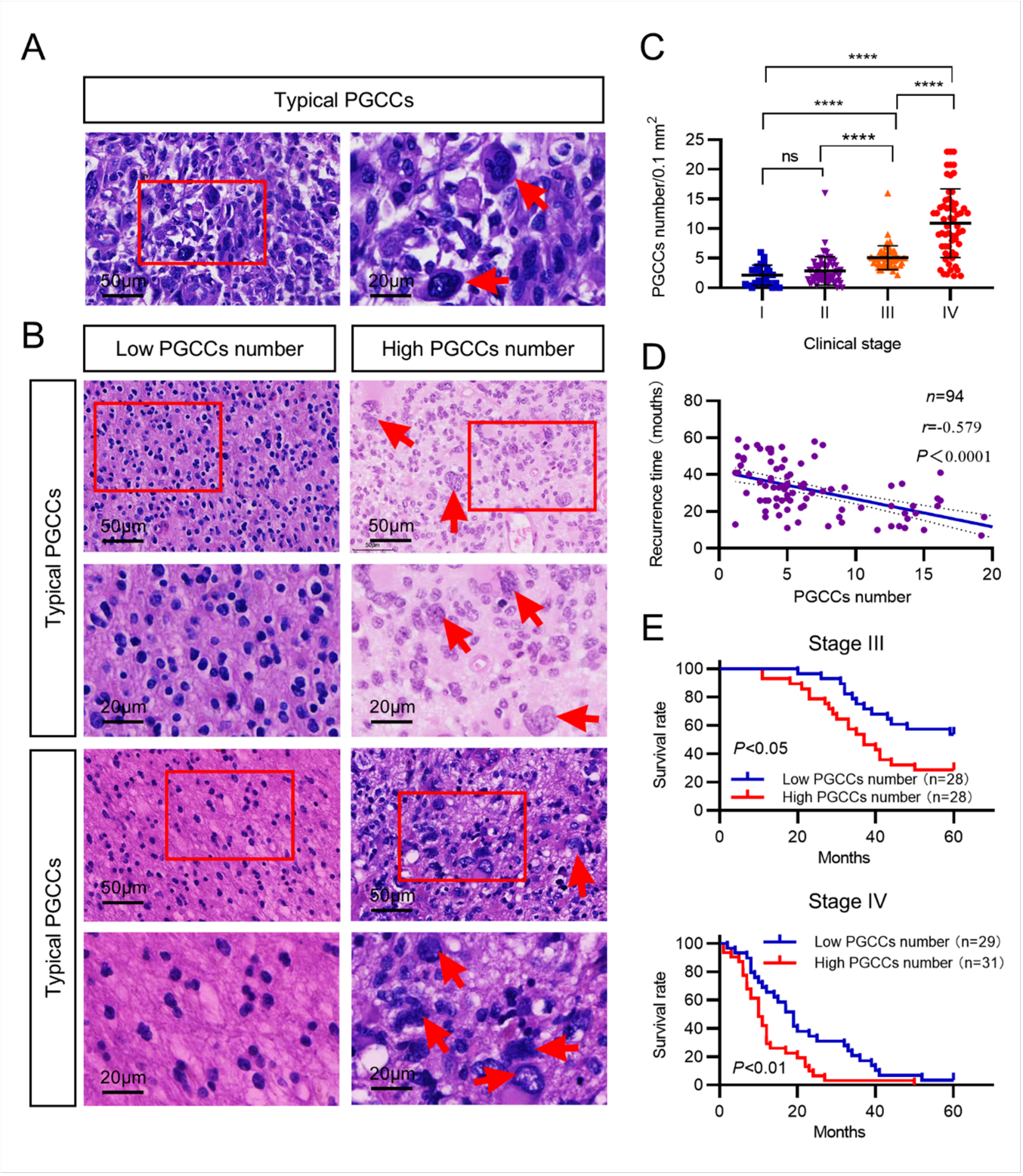


Figure 1

Presence and clinical significance of PGCCs in glioma. (A) Representative H&E staining of typical PGCCs in glioma tissue sections. Identified PGCCs were indicated using the red arrows. (B) Representative images of PGCCs in glioma tissue microarrays. (C) The quantitative analysis of PGCCs across different glioma grades. (D) Pearson correlation between recurrence time and PGCC abundance (linear regression). (E) Kaplan-Meier analysis of 5-year overall survival in patients with grade III and grade

IV glioma stratified by PGCC abundance (log-rank test). Data represent the mean ± SD, ns: no significance, **** $P < 0.0001$.

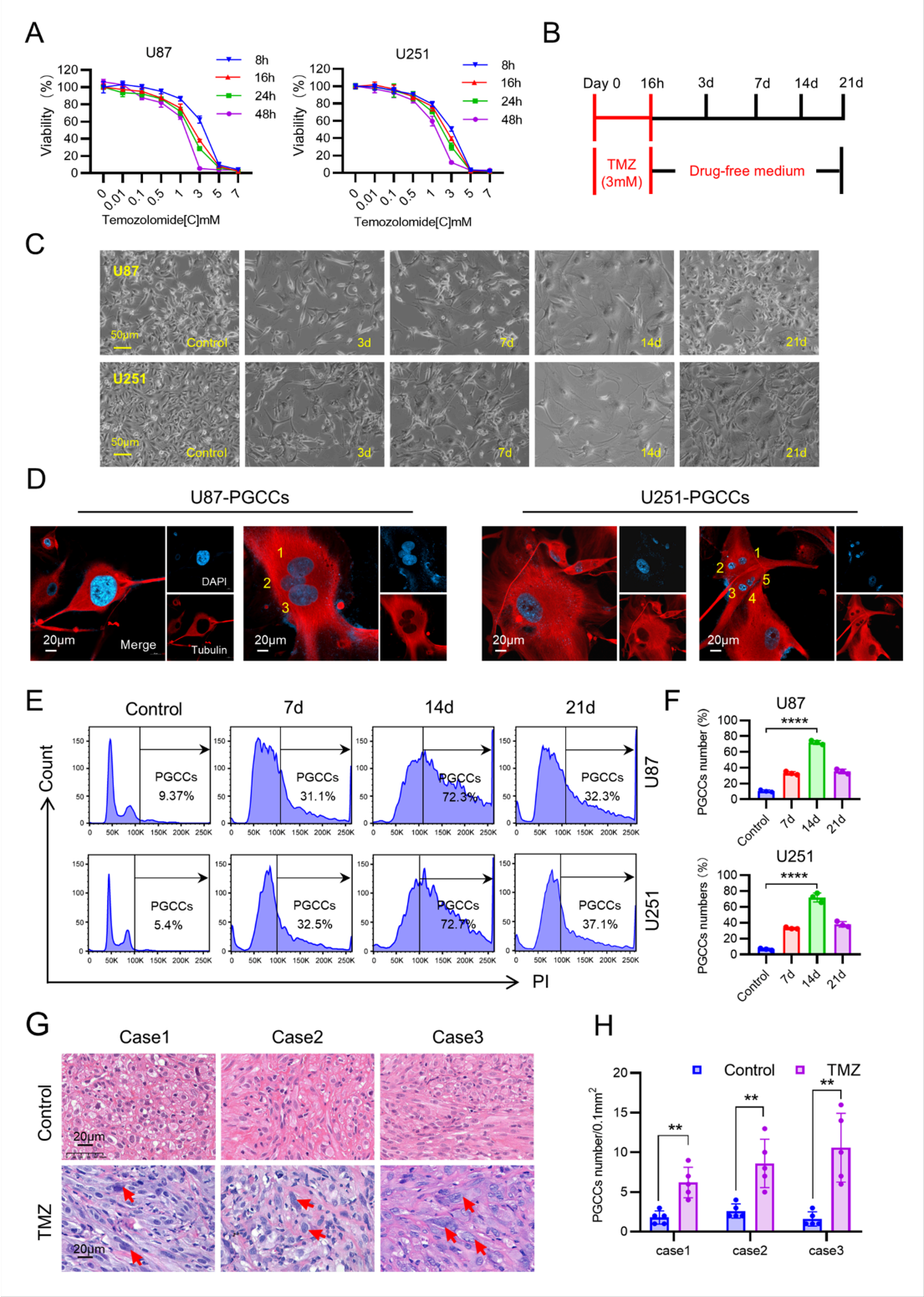


Figure 2

Temozolomide exposure induces the formation of PGCCs both *in vitro* and *in vivo*. (A) CCK-8 assessment of cell viability curves of U87 and U251 cells following exposure to TMZ at the indicated

concentrations. Cell viability were normalized to the corresponding untreated cells at each time point. (B) Schematic illustration of the induction of PGCCs. U87 and U251 cells were treated with 3 mM TMZ for 16h, followed by recovery in regular medium to allow for PGCCs formation. (C) Representative phase-contrast microscopy images showing the morphological changes in U87 and U251 cells before or after TMZ treatment at the indicated periods of time. (D) Immunofluorescence images of morphological features in PGCCs at day 14. Numbers indicate individual nuclei of PGCCs. (E) PI flow cytometry quantification of polyploidy in U87 and U251 cells during TMZ-induced PGCC formation. (F) The bar charts indicate percentage of polyploid cells as quantified by PI staining. (G) H&E staining analysis of PGCC frequency in xenograft tumors with or without TMZ treatment. Arrow indicates representative PGCCs. (H) Statistical analysis of PGCC frequency between vehicle (control) and TMZ-treated xenograft tumors using an unpaired Student's t-test. Data represent the mean ± SD, ** $P < 0.01$, **** $P < 0.0001$.

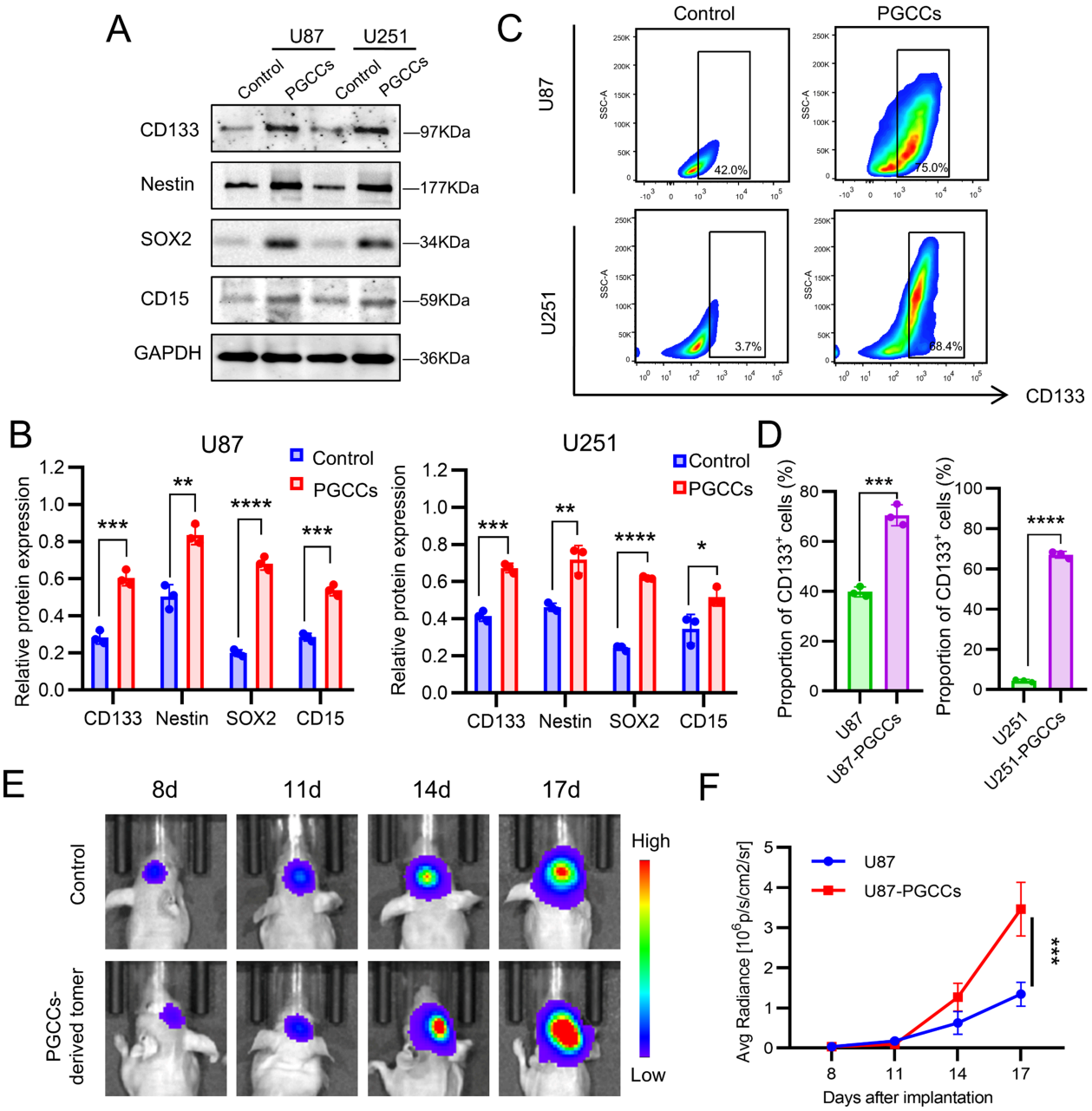


Figure 3

PGCCs exhibit stem cell-like properties. (A) Western blot analysis of glioma stem cell (GSC) marker proteins in parental glioma cells (control) and their derived PGCCs. (B) Quantitative analysis of the expression of GSC marker proteins between control and PGCC U87 and U251 glioma cells. (C) Flow cytometric analysis of the proportion of CD133⁺ cells in parental glioma cells and their derived PGCCs (10,000 events per sample). (D) Quantitative analysis of the proportion of CD133⁺ cells in the indicated groups. (E) Bioluminescent imaging of tumor growth of xenografts derived from U87 and U87-PGCCs. (F) Quantitative analysis of the average bioluminescence intensity of each group using IVIS (n=5). Data represent the mean ± SD, * $P < 0.05$, ** $P < 0.01$, *** $P < 0.001$, **** $P < 0.0001$.

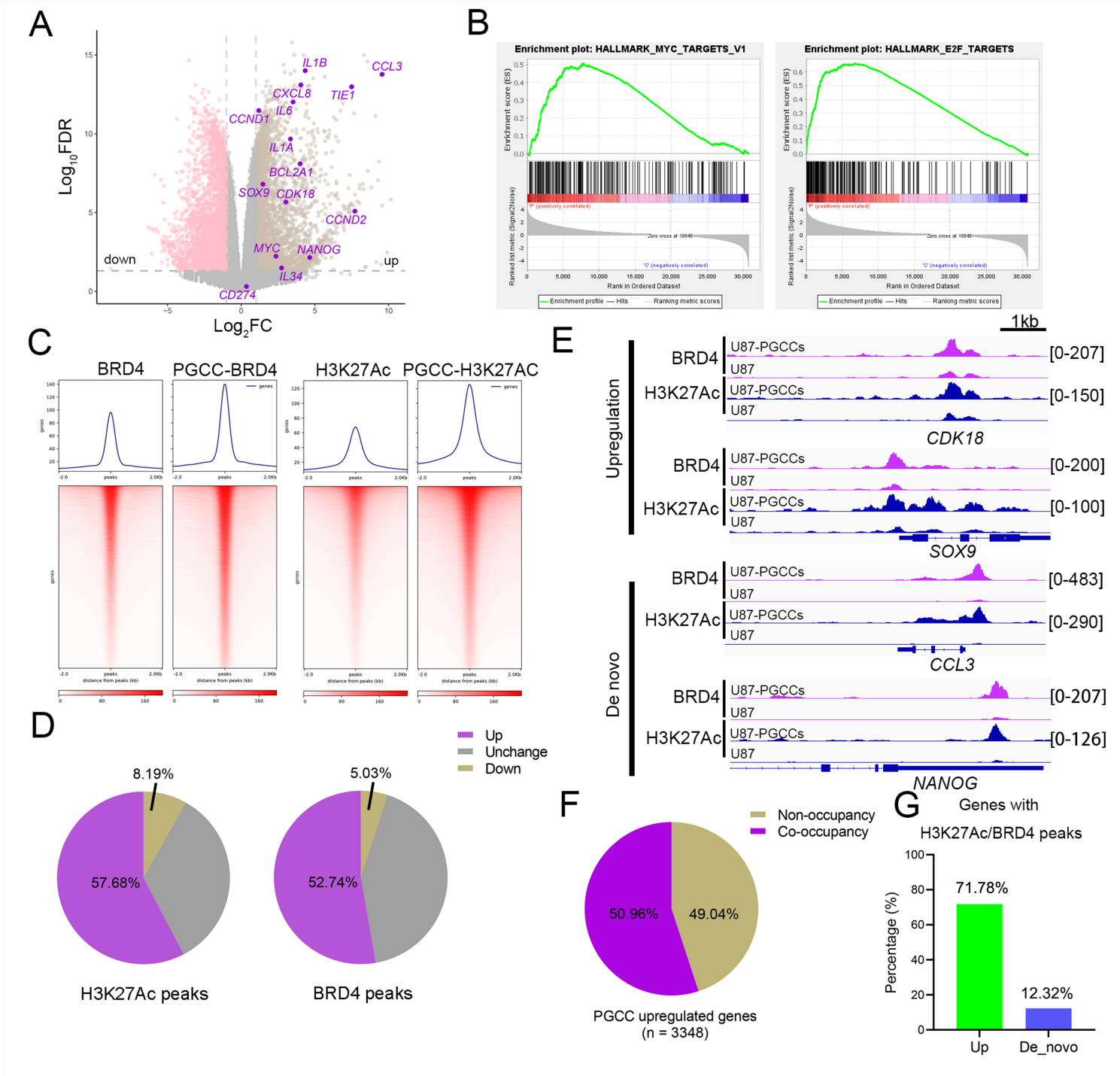


Figure 4

BRD4/H3K27Ac epigenetic reprogramming is linked to PGCC-associated transcriptional profile. (A) Volcano plot of differential gene expression profiles following PGCC formation in U87 cells (cutoff: logFC > 1, FDR < 0.05, n = 5). (B) GSEA of MYC and E2F pathways in PGCCs versus parental cells. (C) Heatmap and density plots showing BRD4 and H3K27Ac peak distributions in PGCCs and parental glioma cells. (D) Pie chart illustrating changes in transcription-level mean scores of BRD4 and H3K27Ac peaks in PGCCs versus parental cells (cutoff: >1.5-fold change). (E) Normalized CUT&Tag tracks of BRD4 and H3K27Ac at representative gene loci. (F) Pie char of the percentage of BRD4/H3K27Ac co-occupancy in

upregulated genes in PGCCs. (G) Bar plot showing the percentage of upregulated genes with gained (>1.5-fold increase), and de novo BRD4/H3K27Ac co-occupancy in PGCCs.

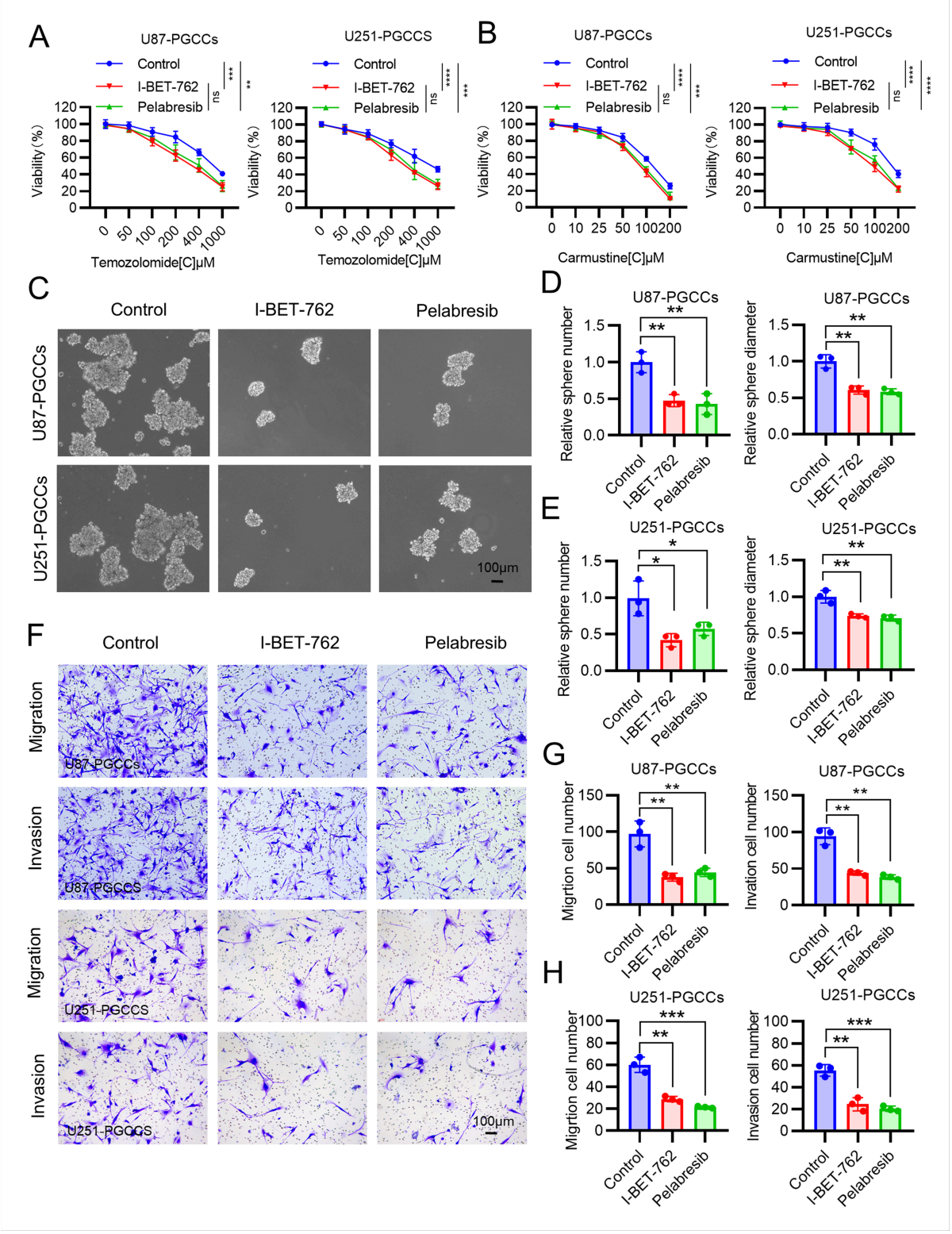


Figure 5

Treatment with BET inhibitors diminishes PGCC-associated chemoresistance, tumorsphere formation and invasiveness. (A) The effect of BET inhibitors I-BET-762 and Pelabresib on cell viability under

different concentrations of TMZ in U87-PGCCs and U251-PGCCs was analyzed by the CCK-8 assay. (B) The effect of BET inhibitors on carmustine sensitivity in U87-PGCCs and U251-PGCCs. (C) Representative light micrographs of tumorsphere formation in U87-PGCCs and U251-PGCCs with or without exposure to BET inhibitors. (D, E) Quantitative analysis of relative sphere number and relative sphere diameter of the indicated groups, U87-PGCCS (D), U251-PGCCS(E). (F) Transwell assay of the effects of BET inhibitors on the migratory and invasive capacities of U87-PGCCs and U251-PGCCs. (G, H) Quantitative analysis of cell migration and invasion of U87-PGCCs (G) and U251-PGCCs (H) cells. Data represent the mean ± SD, ns: no significance, * $P < 0.05$, ** $P < 0.01$, *** $P < 0.001$, **** $P < 0.0001$.

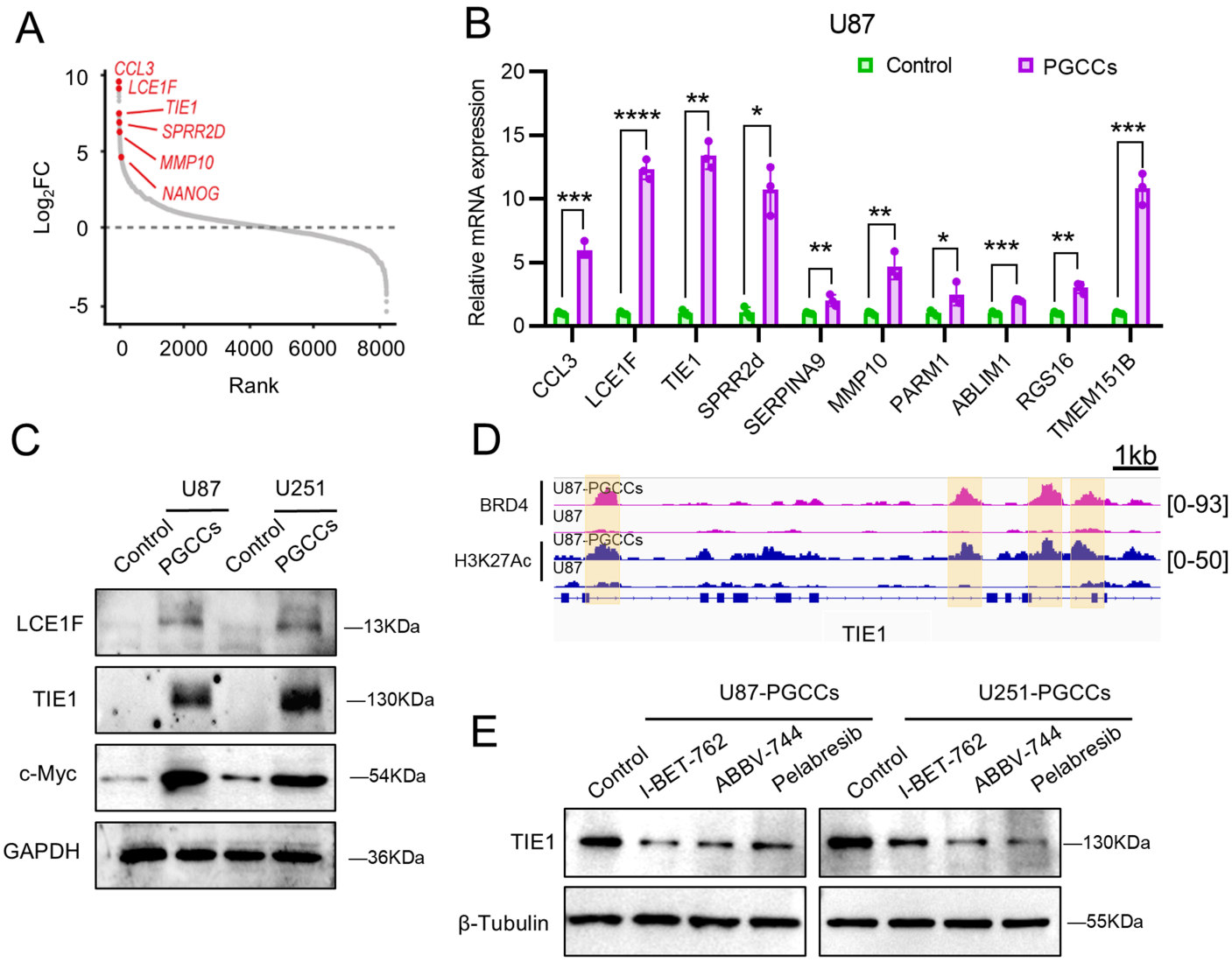


Figure 6

BRD4/H3K27ac-mediated epigenetic reprogramming induces novel oncoprotein expression in PGCCs. (A) Dot plot showing the ranking of logFC values for genes with increased BRD4/H3K27ac co-occupancy in PGCCs. Genes with de novo BRD4/H3K27Ac co-occupancy were highlighted. (B) RT-qPCR verification of upregulated genes in PGCCs versus parental glioma cells (control). (C) Western blot analysis ofthe

indicated proteins in parental glioma cells (control) and PGCCs. (D) CUT&Tag tracks depicting BRD4 and H3K27ac binding profiles across the TIE1 gene locus, with co-occupancy peaks unique to PGCCs highlighted. (E) Western blot analysis of TIE1 expression in PGCCs treatment with or without exposure to BET inhibitors. Data represent the mean ± SD, * $P < 0.05$, ** $P < 0.01$, *** $P < 0.001$, **** $P < 0.0001$

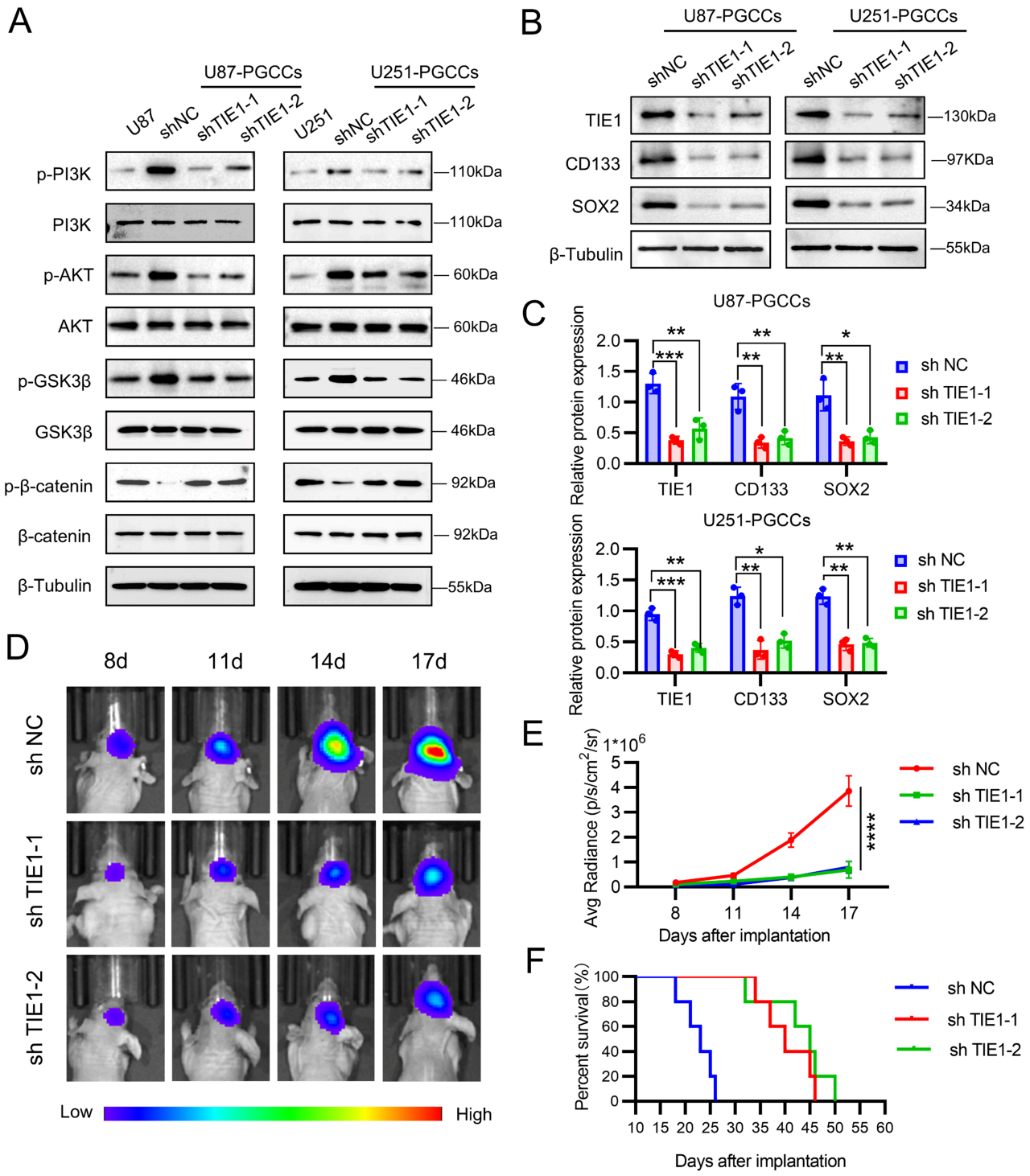


Figure 7

Depletion of TIE1 inhibits the stemness and tumor-propagating capacities of PGCCs. (A) Western blot analysis of PI3K/AKT/GSK3β/β-catenin signaling pathway proteins in U87, U251 and their derived PGCCs with or without knockdown of TIE1. (B) Western blot analysis of TIE1, CD133 and SOX2 in U87-PGCCs and U251-PGCCs cells with or without knockdown of TIE1. (C) Quantitative analysis of the expression of TIE1, CD133 and SOX2. (D) Bioluminescent imaging of tumor growth of xenografts derived from U87-PGCCs expressing shTIE1or shNTC. (E) Quantitative analysis of the average bioluminescence intensity of each group using IVIS (n = 5). (F) Kaplan-Meier survival curves of nude mice harboring U87-PGCCs expressing shTIE1 or shNTC. Data represent the mean ± SD, * $P < 0.05$, ** $P < 0.01$, *** $P < 0.001$, ****P < 0.0001.

Supplementary Files

This is a list of supplementary files associated with this preprint. Click to download.

- SupplementaryTableS1.docx
- SupplementaryTableS2.docx
- fulllengthuncroppedoriginalwesternblots.pdf
- Supplymentaryinformationlegends.docx
- SupplementaryFigure1.tif
- SupplementaryFigure2.tif
- SupplementaryFigure3.tif
- SupplementaryFigure4.tif
- SupplementaryFigure5.tif
- SupplementaryFigure6.tif
- SupplementaryFigure7.tif
- SupplementaryFigure8.tif